

Article

Study on Screening Mechanism and Numerical Simulation for Crashed Concrete Particles by Using DEM

Deyi He  and Chusheng Liu *

China University of Mining and Technology, Xuzhou 221116, China; hedeyi1993@163.com

* Correspondence: liuchusheng@126.com

Abstract: Recycling waste concrete has become a large problem in developing countries. The aim of this work is to provide guidance for screening concrete particles and improving screening efficiency. First, the elastoplastic collision model is established for calculating the coefficient of restitution for concrete particles with different compressive strengths. Then, a bar circular vibrating screen is applied to simulate the screening process of concrete particles by using the discrete element method (DEM). The optimal vibrating parameters, which contain amplitude, frequency and inclination angles, is analyzed for the representative concrete particles containing C15, C45 and C80 by comparing the screening efficiency. The results show that the optimal screening parameters of amplitude and frequency is smaller with the increase in the compressive strength of the concrete particles. Appropriately, the large inclination angle is suitable for screening fine concrete particles with a gap vibrating screen. This work should be helpful for the screening process of concrete waste particles and provides a theoretical basis and simulation case for screening and recycling other particles, such as sand, stone, iron ore and copper ore. In the screening processes of construction wastes, the optimal screening parameters can be selected quickly by calculating the coefficient of restitution and adopting the DEM simulation.

Keywords: waste concrete; discrete element method; the coefficient of restitution; screening efficiency; vibrating screen; hertz contact



Citation: He, D.; Liu, C. Study on Screening Mechanism and Numerical Simulation for Crashed Concrete Particles by Using DEM. *Separations* **2022**, *9*, 153. <https://doi.org/10.3390/separations9060153>

Academic Editor: Qicheng Feng

Received: 2 June 2022

Accepted: 13 June 2022

Published: 14 June 2022

Publisher's Note: MDPI stays neutral with regard to jurisdictional claims in published maps and institutional affiliations.



Copyright: © 2022 by the authors. Licensee MDPI, Basel, Switzerland. This article is an open access article distributed under the terms and conditions of the Creative Commons Attribution (CC BY) license (<https://creativecommons.org/licenses/by/4.0/>).

1. Introduction

Globally, large amounts of concrete produced as a result of demolition cause environmental pollution, additional waste dump and a waste of resources [1]. It has been proved that waste concrete can be recycled as aggregates for reproducing concrete. The physical and mechanical properties of recycled concrete (RC) was earlier studied by Topçu, who examined the 28-day compressive strength of RC and provided the availability of RC [2]. Moreover, the size and replacement ratio of recycled concrete aggregates (RCA) significantly influence compressive strength, split tensile strength, elasticity modulus, abrasion and other indicators [3]. Evangelista [4] studied the mechanical behavior of RC made with different replacement ratios of fine recycled aggregates (FRA) with sizes under 0–5 mm, and gave a reasonable replacement ratio that does not jeopardize the mechanical properties for FRA.

Recycled coarse aggregates can also be raw material for producing RC. An experiment based on different proportions of FRA replacement and fine concrete aggregates (FCA) replacement was implemented by Sérifou [5] and the results show a gradual decrease in compressive, splitting, and flexural strength, with the increase in recycled aggregate percentage. Ly [6] found that concrete-containing FRAs exhibited a higher workability and lower compressive strength than concrete containing natural coarse aggregates, and the particle size distribution (PSD) of FRA can be replaced more freely, depending on the usage of concrete mixtures.

Recently, new methods to test the mechanical properties of RC were developed. Kou [7] used FRA, crashed from fresh concrete, to make partition wall blocks for testing the loss of mass, compressive strength, transverse strength and ultrasonic pulse velocity of the partition blocks. Furthermore, Digital Image Correlation (DIC) has been proved to be a reliable and high-precision method for testing the mechanical properties of RC [8]. Liu [9] analyzed the strain distribution and crack propagation of the modeled concrete containing stone and brick aggregates with the DIC. The X-ray micro-computed tomography scanning technique and image process was used by Duan [10] to measure the mechanical properties and chloride-ion penetration of RC. With the huge amounts of data, the artificial intelligence methods can be used to predict the mechanical properties of RC with high reliability [11].

In chemical properties, Ho [12] assessed the reactions and mechanisms that are involved in various methods, such as the formation of calcium hydroxyapatite, the pozzolanic reaction, and the desulfurization reaction, for confirming the importance of chemical recycling and the use of concrete waste.

These studies present various methodologies for recycling waste concrete. In economics, reuse and recycling strategies are also important for the effective use of concrete wastes and are flexible in regard to lifecycle, the economy and the environment. Guerra [13] proposed algorithms integrated with a 4-Dimensional Building Information Model (4D-BIM) to estimate quantities of concrete and drywall waste generation for on-site reuse and off-site recycling using a temporal-based approach. The proposed algorithms enhance planning and enable the visualization of construction waste performance throughout construction. At the same time, it improved the rate of construction waste reuse and recycling and reduced the raw cost. Mi [14] proposed a new sustainable construction design reflecting the compressive strength ratio effect. This design helped use more original concrete by adjusting the compressive strength ratio according to the requirements of different structures. For considering the lifecycle of RC, calculating and extending recycle times based on concrete usage and life design is important for strategy design. Xia [15] proposes a novel framework to guide the lifecycle assessment (LCA) of concrete structures with reuse and recycling strategies. The framework could help simplify the LCA and give different strategy combinations for improving the reliability. Furthermore, extreme events, such as earthquakes, are highly correlated with the designed structural strength of RC. Welsh-Huggins [16] predicted the lifecycle performance of three concrete mixes under different seismic conditions that benefit LCA and the material choices of waste concretes.

Some researchers found that many other materials, such as municipal solid wastes incineration fly ashes [17], tires [18], carbon fiber reinforced polymer composites, recycled plastic particles [19], can be utilized as raw material for RC in addition to waste concrete.

The above research mainly focuses on the mechanical chemical properties and lifecycle strategies of RC. The processes for concrete waste such as crash and screening also play an important role in recycling concrete waste [20]. Generally, on construction sites, the building process begins with the recycling process. With limited process capacity, building efficiency might be affected by the efficiency of screening. The developed recycling system in many studies [20,21] for concrete waste contain multiple screening processes which cannot be ignored and limit the production of RCA. However, there are few studies concerning the screening mechanisms for concrete waste. A vibrating screen is used as a highly efficient and economic piece of equipment in common screen processes [22–24]. In most cases, the vibrating screen is applied for coal preparation and has become a well-established technology. The experimental method is a classical method for studying the screening mechanisms of coal preparation with high reliability [25]. However, testing takes a significant amount of time and the results cannot be used in other situations. For these reasons, a simulation method called the discrete element method is developed for screening granular materials [26,27], such as coal [28], iron ore [29] and copper ore [30]. In the present study, the discrete element method is proved to be an important method for revealing the mechanism of coal screening.

Although coal screening technology is relatively mature, there remain some important issues. The screening mechanisms for different particles is not discussed. Due to the different parameters of the particles, an optimal screening method might be completely different. Hertz [31] first proposed the elastic model of two contact elastic particles which calculate the contact force between two particles. Based on his research, the coefficient of restitution between two particles and between particles and the screening surface can be calculated, which is ignored by most researchers in their studies on particle screening. With the calculated parameters, the screening mechanisms of different types of concrete can be explored. Additionally, this content will be explained in next section. The suitable screening parameters for different concrete wastes is variable because the mechanical parameters of concrete with different standards or batches are different.

The aim of this research is to reveal the screening mechanisms of different concrete wastes. First, a dynamic model of particle collisions is established to calculate the coefficient of restitution of concrete particles based on the Hertz contact model. Then, a bar screen is used for FRAs screening, and the DEM simulation is carried out by screening three types of FRAs. Finally, the optimal screening parameters are given for different types of concrete.

2. Basic Theory

2.1. The Elastoplastic Collision Model of Two Particles and Rigid Plate

Hertz [31,32] deduced the contact force of two elastic particles with radius R_1 and R_2 using the elastic mechanical method. The elastoplastic collision model contains two different types of deformation areas during the collision between particles and the vibrating screen, as shown in Figure 1. The elastic contact area obeys the law of Hertz contact theory, and the plastic contact area appears when the stress reaches the compressive strength of the material. The stress distribution is shown in Figure 1. In the period of the elastic collision, the contact radius r_a under a load P_0 is given by

$$r_a^3 = \frac{3}{4} \pi (k_1 + k_2) \frac{R_1 R_2}{R_1 + R_2} P_0 \tag{1}$$

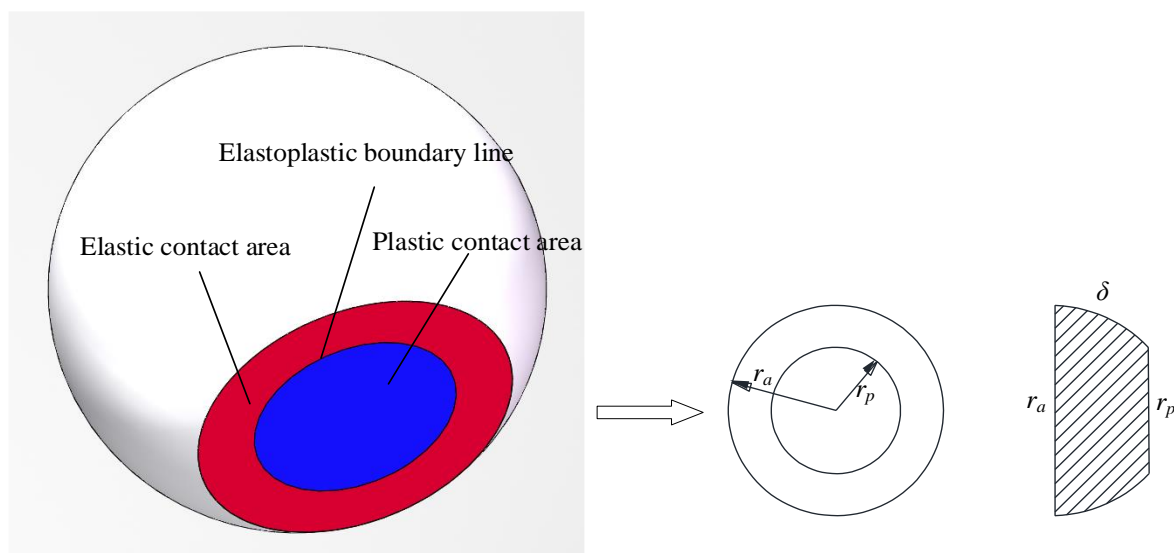


Figure 1. The elastoplastic collision model of particles.

In which k_1 and k_2 are the elastic constants of the particles. That is

$$k_1 = \frac{1 - \mu_1^2}{\pi E_1} \tag{2}$$

$$k_2 = \frac{1 - \mu_2^2}{\pi E_2} \tag{3}$$

where μ is the Poisson ratio and E is the Young modulus of each particles

$$\delta^3 = \frac{9}{16} \pi^2 (k_1 + k_2)^2 \frac{R_1 + R_2}{R_1 R_2} P_0^2 \tag{4}$$

where δ is relative deformation of two particles. Now, force

$$E = \frac{1}{\pi(k_1 + k_2)} \tag{5}$$

$$R = \frac{R_1 R_2}{R_1 + R_2} \tag{6}$$

Combining (1), (4)–(6), that is

$$r_a = \left(\frac{3P_0 R}{4E} \right)^{\frac{1}{3}} \tag{7}$$

$$\delta = \frac{3P_0}{4Er_a} \tag{8}$$

In addition, there are

$$r_a^2 = R\delta \tag{9}$$

$$P_0 = \frac{4}{3} E \sqrt{R} \delta^{\frac{3}{2}} \tag{10}$$

For the collision of two particles, the dynamic equations can be expressed as

$$m_1 \frac{d^2 \delta_1}{dt^2} = P_0 \tag{11}$$

$$m_2 \frac{d^2 \delta_2}{dt^2} = P_0 \tag{12}$$

In which the total deformation can be added by each particle deformation, that is

$$\frac{d^2 \delta}{dt^2} = \frac{d^2 \delta_1}{dt^2} + \frac{d^2 \delta_2}{dt^2} \tag{13}$$

Combining Equations (11)–(13) gives

$$m \frac{d^2 \delta}{dt^2} = P_0 = \frac{4}{3} E \sqrt{R} \delta^{\frac{3}{2}} \tag{14}$$

where m is the equivalent mass of two particles

$$m = \frac{m_1 m_2}{m_1 + m_2} \tag{15}$$

According to the Hertz contact theory, the stress distribution of a deformed circular area is given by

$$\sigma(r) = \frac{2E}{\pi R} \sqrt{r_a^2 - r^2} \tag{16}$$

Therefore, the stress of the contact area center is given by

$$\sigma_{\max} = \frac{2Er_a}{\pi R} \tag{17}$$

In the elastic collision period, the max stress of the contact area is the yield strength of the particle material, which is equal to the compressive strength of waste concrete. Therefore, the critical contact radius of the elastic collision period can be expressed as

$$r_{a1} = \frac{\pi R \sigma_s}{2E} \tag{18}$$

σ_s is the compressive strength of waste concrete. Therefore, the critical deformation is given by

$$\delta_1 = R \left(\frac{\pi \sigma_s}{2E} \right)^2 \tag{19}$$

The dynamic Equation (14) can be solved by using the separate variable method with the boundary conditions (when $\delta = 0$, the speed $\dot{\delta} = v_0$), and the relative velocity of two particles is given by

$$\dot{\delta} = \sqrt{(v_0)^2 - \frac{16E\sqrt{R}}{15m} \delta^{\frac{5}{2}}} \tag{20}$$

Equation (19) gives the critical deformation, therefore the velocity at the end of elastic collision is given by

$$v_1 = \sqrt{(v_0)^2 - \frac{16E\sqrt{R}}{15m} \delta_1^{\frac{5}{2}}} \tag{21}$$

With the increase in contact force, the plastic contact area appears in the central contact area and gradually expands. At this collision moment, the elastic contact area becomes a ring and wraps round the plastic contact area.

$$P_2 = \int_{r_p}^{r_a} \int_0^{2\pi} \frac{2Er}{\pi R} \sqrt{r_a - r^2} d\theta dr = \frac{4E(r_a^2 - r_p^2)^{1.5}}{3R} \tag{22}$$

In the elastic-plastic collision period, the maximum stress is the compressive strength of concrete and is located in the plastic sphere contact area. According to the edge of the plastic contact area, considering Equation (14), the compressive strength can be given by

$$\sigma_s = \frac{2E}{\pi R} \sqrt{r_a^2 - r_p^2} \tag{23}$$

Combining (22), (23), there are

$$P_2 = \frac{\pi^3 R^2 \sigma_s^3}{6E^2} \tag{24}$$

Moreover, the total contact force can be expressed as

$$P_2 = \frac{\pi^3 R^2 \sigma_s^3}{6E^2} + \pi r_p^2 \sigma_s \tag{25}$$

Furthermore, Combining (22)–(25)

$$P_2 = \pi \sigma_s R \delta - \frac{\pi^3 R^2 \sigma_s^3}{12E^2} \tag{26}$$

Finally, the dynamic equations in the plastic contact period are written as

$$m \frac{d^2 \delta}{dt^2} = - \left(\pi \sigma_s R \delta - \frac{\pi^3 R^2 \sigma_s^3}{12E^2} \right) \tag{27}$$

The relative speed of two particles in the plastic contact period can be calculated combined with boundary conditions (when $\delta = \delta_1, \dot{\delta} = \dot{\delta}_1$)

$$\dot{\delta} = \sqrt{\dot{\delta}_1^2 - \frac{\pi^5 R^3 \sigma_s^5}{48mE^4} + \frac{\pi^3 R^2 \sigma_s^3}{6mE^2} \delta - \frac{\pi R \sigma_s}{m} \delta^2} \tag{28}$$

In the end of the plastic contact period, the relative speed becomes 0. Therefore, relative deformation can be calculated by using Equation (28), which is given by

$$\delta_2 = \sqrt{\left(\frac{\pi^2 R \sigma_s^2}{6mE^2}\right)^2 + \frac{m \dot{\delta}_1^2}{\pi R \sigma_s} + \frac{\pi^2 R \sigma_s^2}{12E^2}} \tag{29}$$

The last period is the elastic recover period. In this period, the two particles separated from each other and the restoring force at the beginning is equal to the contact force at the end of the plastic contact period. Therefore, the restoring force can be given by

$$P_2 = \frac{4}{3} E \sqrt{R} (\delta - \delta_p)^{\frac{3}{2}} \tag{30}$$

The restoring force at the beginning of this period is equal to the contact force at the end of the plastic contact period, and there are

$$\pi \sigma_s R \delta_2 - \frac{\pi^3 R^2 \sigma_s^3}{12E^2} = \frac{4}{3} E \sqrt{R} (\delta_2 - \delta_p)^{1.5} \tag{31}$$

So, the δ_p is expressed as

$$\delta_p = \delta_2 - \left[\frac{3}{4E\sqrt{R}} \left(\pi \sigma_s R \delta_2 - \frac{\pi^3 R^2 \sigma_s^3}{12E^2} \right) \right]^{\frac{2}{3}} \tag{32}$$

The dynamic equations can be established in the same way

$$m \frac{d^2 \delta}{dt^2} = P_2 = \frac{4}{3} E \sqrt{R} (\delta - \delta_p)^{\frac{3}{2}} \tag{33}$$

The dynamic Equation (33) can be solved by using the separate variable method with the boundary conditions (when $\delta = \delta_2$, the speed $\dot{\delta} = 0$), and the separated velocity of two particles is given as

$$\dot{\delta} = -\sqrt{\frac{16E\sqrt{R}}{15m} (\delta_2 - \delta_p)^{\frac{5}{2}} - \frac{16E\sqrt{R}}{15m} (\delta - \delta_p)^{\frac{5}{2}}} \tag{34}$$

At the end of the elastic recover period, we have $\delta = \delta_p$, and the relative velocity is given as

$$v_3 = -\sqrt{\frac{16E\sqrt{R}}{15m} (\delta_2 - \delta_p)^{\frac{5}{2}}} \tag{35}$$

Finally, the coefficient of restitution is given

$$e = \left| \frac{v_3}{v_0} \right| \tag{36}$$

2.2. The Restitution Process between Particles and Screen Surface

In this process, we consider young's modulus and the compressive stress of the screening surface, which is made of iron and is far larger than concrete, so the screening

surface can be considered a rigid body. So, the radius and mass of the screening surface is infinite and compared to (6) and (15), we have

$$R = \frac{R_1 R_2}{R_1 + R_2} = R_1 \tag{37}$$

$$m = \frac{m_1 m_2}{m_1 + m_2} = m_1 \tag{38}$$

In which R_1 and m_1 is the radius and the mass of the particle. These two parameters differ from the elastoplastic collision model of two particles and the other calculation process is the same.

2.3. Calculation of Coefficient of Restitution for Concrete Particles

We selected three typical types of concrete with different compressive strength levels for the screening simulation. The parameters of these concretes are presented in Table 1.

Table 1. The mechanic parameters of chosen concrete.

	C15	C45	C80
Density	2360	2410	2440
Poisson’s ratio	0.17	0.17	0.17
Elastic modulus (GPa)	22	33.5	38
Compressive strength	15	45	80

Therefore, the restitution coefficient of these concretes can be calculated under the above method. Figure 2 shows the relationship between the particle speed and restitution coefficients with the chosen concretes.

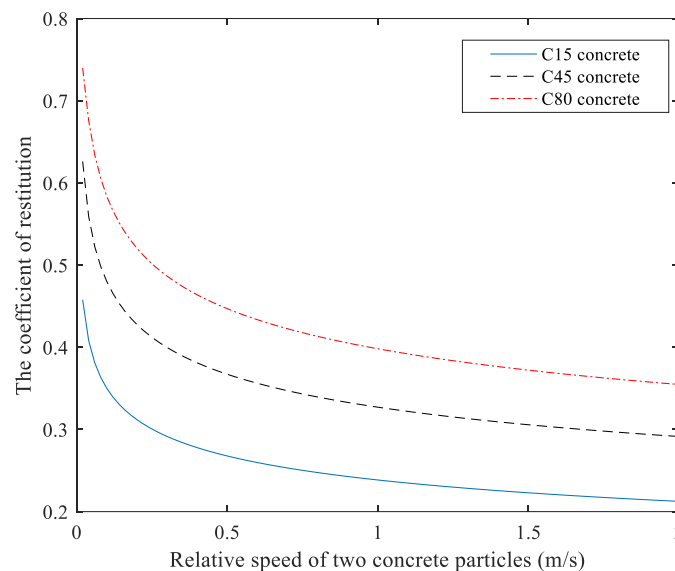


Figure 2. The relation between particles speed and restitution coefficients with the chosen concretes.

As shown in the figure, the restitution coefficient of the concrete particles is highly correlated with the compressive strength level. The higher the compressive strength, the higher the restitution coefficient. The coefficient of the restitution decreases with the relative speed of two concrete particles due to the nonlinear characteristic of the Hertz contact. In other research, the coefficient of restitution is set up as a constant, which was not calculated using different particle mechanical parameters [20]. However, this parameter would affect the screening process of concrete and other particles. Obviously, the particles

would bounce higher with a high restitution coefficient. Therefore, the screening efficiency will be influenced by the restitution coefficient.

Moreover, it was found that the coefficient of restitution decreased with the relative speed, and a nonlinear relationship existed between them. That is because the plastic deformation became larger with the increase in the relative speed and a nonlinear relationship existed between them.

Figure 3 shows the relationship between the particle radius and the coefficient of restitution of C80 concrete. It was found that the coefficient of restitution decreased slightly with the increase in the radius of the concrete particles, and the relationship is nonlinear. The radius of concrete particles can be ignored for calculating the coefficient of restitution because the coefficient of restitution is hardly affected by the particle radius.

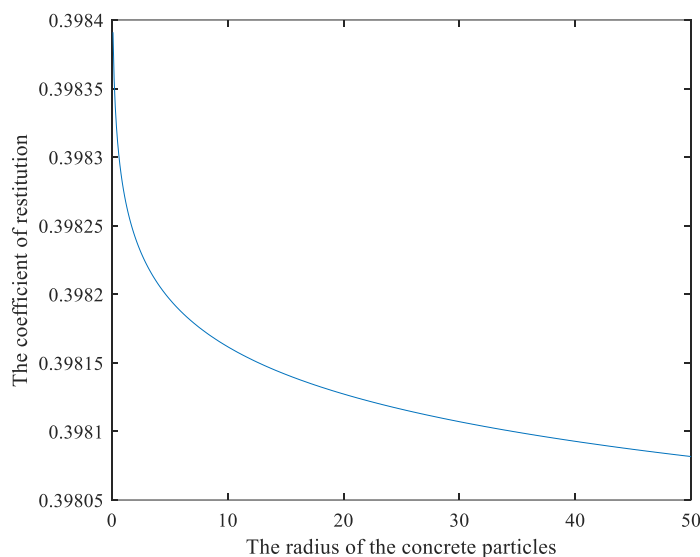


Figure 3. The relation between the particle radius and the coefficient of restitution.

Normally, the amplitude of the vibrating screen is 4–6 mm, and the frequency is about 16 Hz. For the convenience of calculating the coefficient of restitution, we take the relative velocity as 1 m/s.

3. Simulation Conditions

Figure 4 shows the CAD model of the circular vibrating screen and the main section is marked. The circular vibrating screen is forced by one motor and the motion path is circular. The detailed screening parameters are shown in Table 2. Table 3 shows the particle material parameters of the used concrete.

Table 2. The screening and operational parameters used in the experiments.

Parameters	Value
Screen length (mm)	600
Screen width (mm)	300
Bar gap (mm)	5
Bar diameter (mm)	5
Particle size range (mm)	3–5 5–10
Mass of feeding materials for each particle size range in an experiment (kg/s)	3.5 3.5
Total feeding rate (kg/s)	7
Inclination angle of the deck α ($^{\circ}$)	15, 20, 25, 30
Vibration frequency f (Hz)	12, 14, 16, 18
Vibration amplitude A (mm)	2, 3, 4, 5
Vibration motion	Circular

Table 3. Particle material parameters of C15, C45, C80 concrete used in the simulations.

Parameters	Value		
	C15	C45	C80
Coefficient of restitution for particle to particle	0.2385	0.3271	0.3982
Coefficient of static friction	0.5	0.5	0.5
Coefficient of rolling friction	0.01	0.01	0.01
Coefficient of restitution for particle to screening surface	0.2125	0.2915	0.3548
Coefficient of static friction	0.4	0.4	0.4
Coefficient of rolling friction	0.01	0.01	0.01

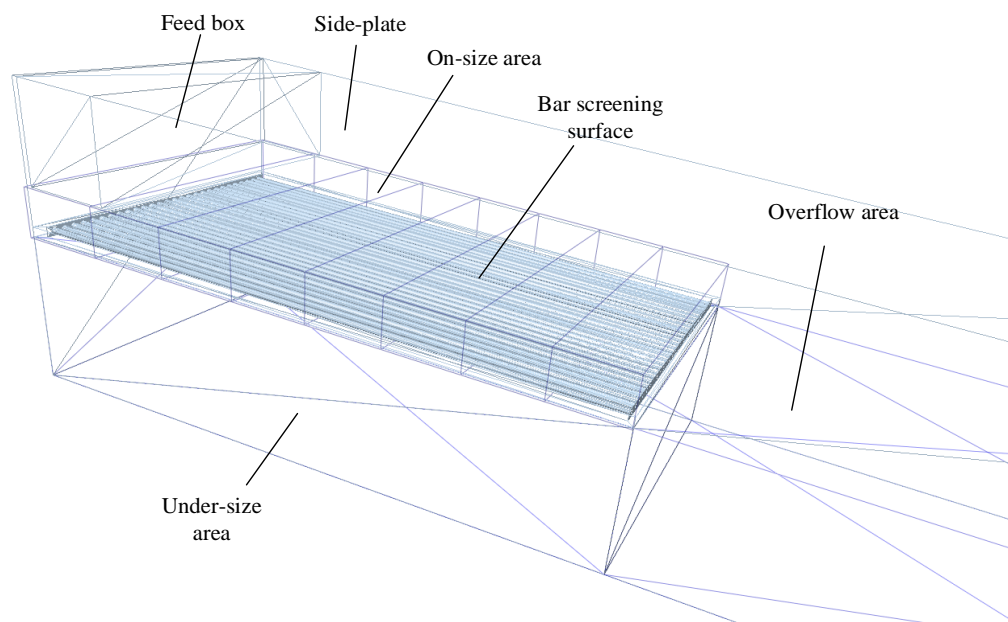


Figure 4. The CAD model of the circular vibrating screen.

4. Results and Discussion

The DEM simulations were performed based on the CAD model and the above settings. Additionally, the commercial software package of EDEM 2018 was employed to simulate the screening process of the concrete particles with a bar screen. The simulation time step was set to be 1×10^{-6} s, which is smaller than the Rayleigh time step calculated by EDEM. Moreover, the total simulation time was set to 5 s and the particles reached a stable state in the screening process, which means the real time screening efficiency and particles motion state became stable.

4.1. The Simulation Analysis for a Typical Screening Process

At the beginning of the screening process, the concrete particles generate in the feed box and fall to the screening surface freely. The concrete particles bounce and fall from the onsite area to the overflow area under the gravity and vibration of the screening surface. In this process, the fine concrete particles have the opportunity to go through the screening surface gap at each bounce moment. The coarse concrete particles are conveyed to the overflow area. With the screening of the concrete particles, the contents of fine concrete particles decreases, and part of fine concrete particles are conveyed to the overflow area. The less fine concrete particles in the overflow area, the higher the screening efficiency.

Figure 5 shows a snapshot of the screening process for concrete particles. The red particles are fine concrete particles, and the blue particles are coarse concrete particles.

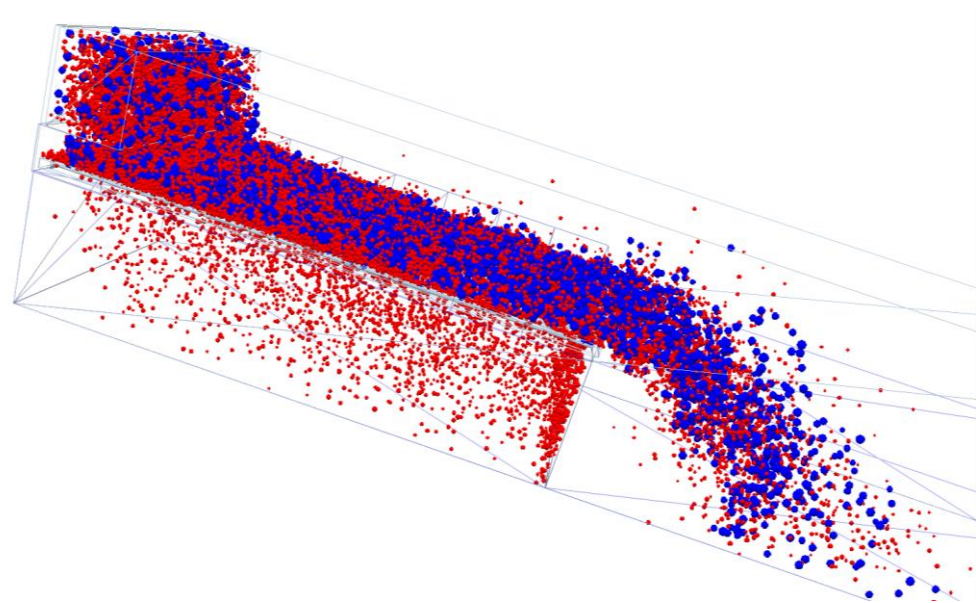


Figure 5. The screening process of the concrete particles.

In Figure 6, the mass of fine concrete particles along with the length of the screening surface is presented. The screening area is divided into eight parts according to the length of the screening surface. Furthermore, the mass of fine concrete particles in each part is recorded. As the figure shows, the particles cover the screening surface in about 1.4 s and keep in a stable screening state.

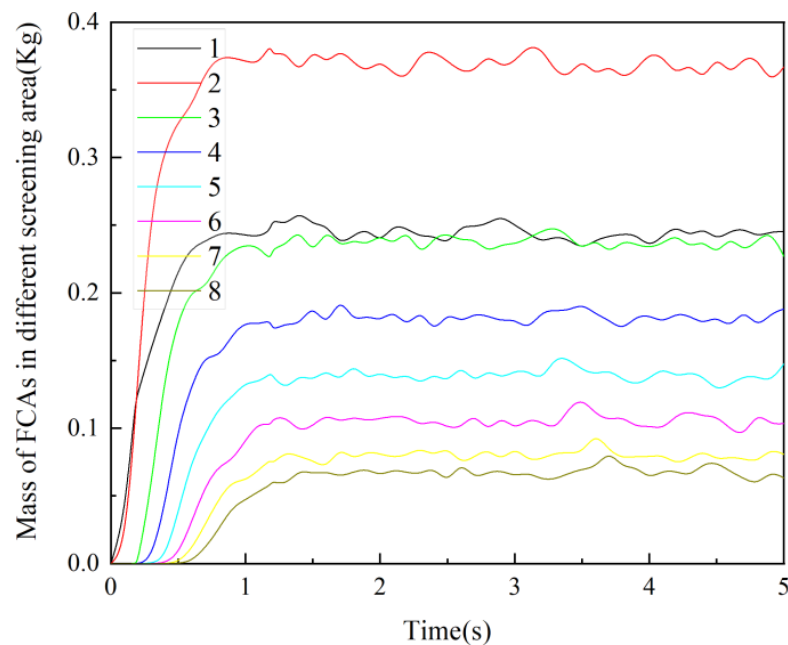


Figure 6. The particles distribution on screening surface.

Basically, with the screening process, the mass of fine concrete decrease with the length of the screening surface; the closer to the end of the overflow area the less content of the fine concrete. Moreover, the mass of area 1 is less than area 2 and the particles cannot cover area 1 due to the gravity. Obviously, the screening capacity is gradually decreased with the decrease in distance to the overflow area. This shows the screening process of the concrete particles.

4.2. Optimal Parameters for Different Concretes

We applied the orthogonal for screening concrete particles. Furthermore, three vibrating parameters (amplitude, frequency and inclination angle) were selected to optimize screening efficiency. Additionally, the parameters of the vibrating screen were adjusted to optimize screening efficiency [27–29]. Moreover, a pre-simulation was completed for choosing appropriate factors. Based on the vibrating parameters, four factors and three levels of simulation tests are listed in Table 4.

Table 4. The orthogonal test date for concrete particles screening.

Case Number	Amplitude	Frequency	Inclination Angle	Screening Efficiency (%)		
				C15	C45	C80
1	2	12	15	36.8	38.1	44.7
2	2	14	18	40.2	44.3	52.7
3	2	16	21	49.1	52.7	57.4
4	2	18	24	54.7	43.2	60.2
5	3	12	18	58.4	66.5	78.2
6	3	14	15	65.5	70.9	82.2
7	3	16	24	72.5	78.2	84.1
8	3	18	21	70.6	80.5	83.7
9	4	12	21	78.9	80.2	77.2
10	4	14	24	78.2	79.7	75.3
11	4	16	15	81.6	76.8	73.5
12	4	18	18	78.5	73.2	68.2
13	5	12	24	77.2	71.3	65.2
14	5	14	21	68	65.8	61.3
15	5	16	18	65.3	62.1	55.8
16	5	18	15	62.4	60.4	53.2

Table 4 shows that the screening efficiency is quite small when the amplitude is 2 mm, and the screening efficiency increases with the increase in frequency and inclination angle. The concretes particles pile up on the screening surface because the smaller the amplitude and the frequency the smaller the vibration intensity. Moreover, the particles with larger coefficient of restitution will bounce higher on the screening surface with the same vibrating conditions. Therefore, the screening efficiency of concrete particles with higher compressive strength is higher as well.

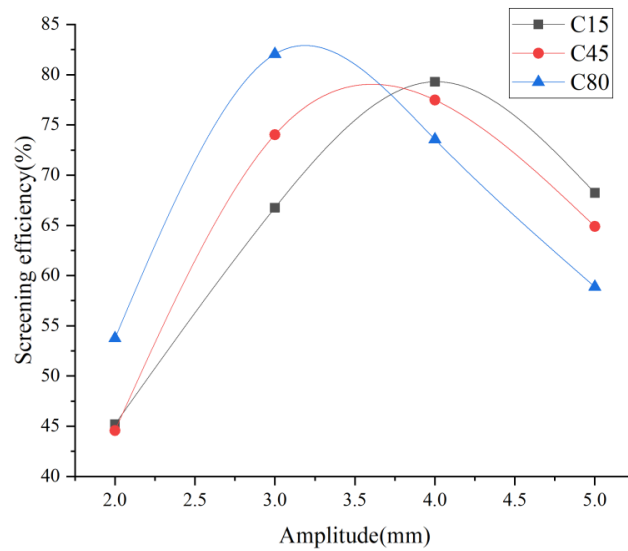
Figure 7 shows the effects of the amplitude, frequency and inclination angle of the vibrating screen on the average screening efficiency for different concrete particles based on the calculated screening efficiency list in Table 4. As shown in Table 4, the average screening efficiency is calculated by the factors of each amplitude level.

Figure 7a shows the influence of the amplitude level on screening efficiency of different concrete particles. The screening effect of particles with higher compressive strength is better in low amplitude condition. Moreover, the screening effect of particles with lower compressive strength is better in larger amplitude condition. The amplitude for the best screening effect of C15, C45 and C80 concrete particles is 4, 4 and 3 mm, and it can be deduced that the optimal screening amplitude of C45 concrete particles is between 3 and 4 mm. Therefore, it can be expressed that the optimal amplitude decreases with the increase in the coefficient of restitution. In conclusion, the appropriate amplitude should be selected according to the coefficient of restitution of particles, and a smaller amplitude should be used with the increase in coefficient of restitution of chosen particles.

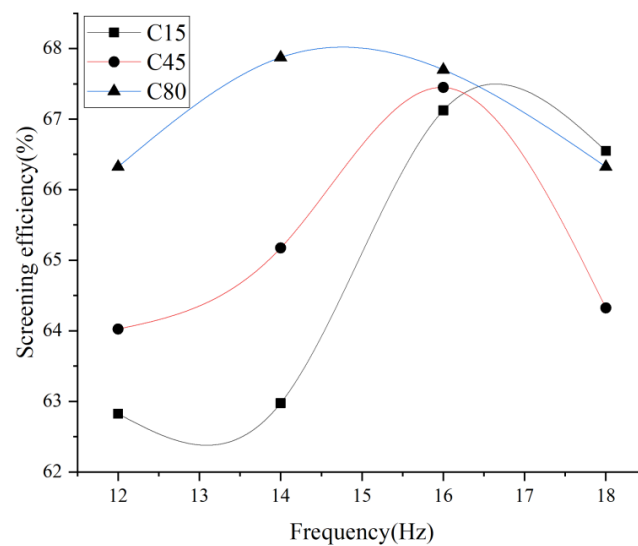
Figure 7b shows the effects of the frequency of the vibrating screen on the average efficiency. It can be seen that the screening efficiency of particles with higher compressive strength in low frequency is better. The optimal frequency of all concrete particles is about 16 Hz and the optimal frequency of particles with higher compressive strength is slightly smaller than particles with lower compressive strength. This is because a high frequency is

beneficial to particle stratification and particles with lower compressive strength need a bigger frequency.

Figure 7c shows the relationship between the inclination angle and average screening efficiency. The screening efficiency under a larger inclination angle is higher because the equipment capacity of the bar screen is large and a larger inclination angle is beneficial to the spread of particles.

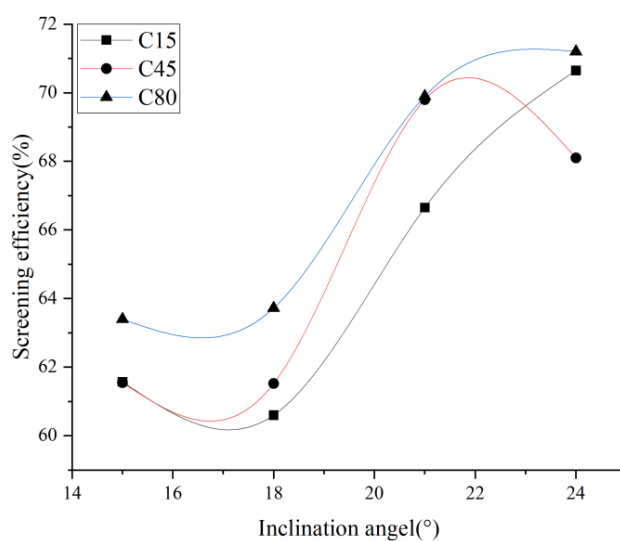


(a)



(b)

Figure 7. Cont.



(c)

Figure 7. The effects of vibration parameters on the average screening efficiency. (a) the effects of amplitude on the average screening efficiency; (b) the effects of frequency on the average screening efficiency; (c) the effects of inclination angle on the average screening efficiency.

5. Conclusions

A collision model of particles was conducted based on Hertz contact and dynamic analysis. The coefficient of restitution for concrete particles with different compressive level was calculated. Moreover, the DEM simulation with a circular bar screen was completed for screening concrete particles using an orthogonal experimental design. The combined effects of the vibration parameters of amplitude, frequency and inclination angle on screening efficiency was analyzed for comparing the optimal parameters of different concrete particles. The following conclusions can be drawn from the present study:

(1) The restitution coefficient of the concrete particles is highly correlated with the compressive strength level and the higher the compressive strength the higher the restitution coefficient. The effects of particle radius can be ignored when calculating the restitution coefficient.

(2) The optimal screening parameters of amplitude and frequency is smaller with the increase in the compressive strength of concrete particles. Appropriately, the large inclination angle is suitable for screening fine concrete particles with a gap vibrating screen.

In this manuscript, we provide a pervasive simulation process for screening concrete particles, which is also suitable for screening other granular materials. The optimal screening parameters can be selected quickly by calculating the coefficient of restitution and adopting the DEM simulation in the screening processes of other granular materials. In future studies, the screening experiment of concrete particles will be necessary for verifying the reliability of the screening simulation. Other construction wastes, such as bricks, stones, sands, etc., should also be considered for revealing the screening mechanism and improving screening efficiency, which will be beneficial for concrete batching, recycling waste and improving the mechanical properties of building material.

Author Contributions: Conceptualization, D.H. and C.L.; methodology, D.H. and C.L.; software, D.H.; validation, D.H.; formal analysis, D.H.; investigation, D.H.; resources, D.H. and C.L.; data curation, D.H.; writing—original draft preparation, D.H.; writing—review and editing, D.H. and C.L.; visualization, D.H.; supervision, D.H.; project administration, C.L.; funding acquisition, C.L. All authors have read and agreed to the published version of the manuscript.

Funding: The research presented in this work was funded by the National Natural Science Foundation of China [51775544] and Xuzhou XCMG Mining Machinery CO.LTD [2020050049-07].

Data Availability Statement: The data is available to contact the author (hedeyi1993@163.com).

Conflicts of Interest: The authors declare no conflict of interest.

References

1. Akhtar, A.; Sarmah, A.K. Construction and demolition waste generation and properties of recycled aggregate concrete: A global perspective. *J. Clean Prod.* **2018**, *186*, 262–281. [\[CrossRef\]](#)
2. Topçu, I.B. Physical and mechanical properties of concretes produced with waste concrete. *Cem. Concr. Res.* **1997**, *27*, 1817–1823. [\[CrossRef\]](#)
3. Guo, L.; Guan, Z.; Guo, L.; Shen, W.; Xue, Z.; Chen, P.; Li, M. Effects of Recycled Aggregate Content on Pervious Concrete Performance. *J. Renew. Mater.* **2020**, *8*, 1711–1727. [\[CrossRef\]](#)
4. Evangelista, L.; Brito, J.D. Mechanical behaviour of concrete made with fine recycled concrete aggregates. *Cement Concrete Compos.* **2007**, *29*, 397–401. [\[CrossRef\]](#)
5. Sérifou, M.; Sbartai, Z.M.; Yotte, S.; Boffoué, M.O.; Emeruwa, E.; Bos, F. A Study of Concrete Made with Fine and Coarse Aggregates Recycled from Fresh Concrete Waste. *J. Constr. Eng.* **2013**, *2013*, 317182. [\[CrossRef\]](#)
6. Ly, B.T.; Far, H. Investigation on properties of coarse reclaimed aggregates and their effects on concrete strength and workability. *Struct Concr.* **2019**, *20*, 1622–1630. [\[CrossRef\]](#)
7. Kou, S.C.; Zhan, B.J.; Poon, C.S. Properties of partition wall blocks prepared with fresh concrete wastes. *Constr Build. Mater.* **2012**, *36*, 566–571. [\[CrossRef\]](#)
8. Zhang, L.W.; Sojobi, A.O.; Liew, K.M. Sustainable CFRP-reinforced recycled concrete for cleaner eco-friendly construction. *J. Clean Prod.* **2019**, *233*, 56–75. [\[CrossRef\]](#)
9. Liu, Q.; Xiao, J.; Singh, A. Crack Propagation and Failure Characteristics of Modeled Concrete with Natural and Brick Aggregates. *J. Renew. Mater.* **2021**, *9*, 19. [\[CrossRef\]](#)
10. Duan, Z.; Han, N.; Singh, A.; Xiao, J. Multi-Scale Investigation on Concrete Prepared with Recycled Aggregates from Different Parent Concrete. *J. Renew. Mater.* **2020**, *8*, 1375–1390. [\[CrossRef\]](#)
11. Gholampour, A.; Mansouri, I.; Kisi, O.; Ozbakkaloglu, T. Evaluation of mechanical properties of concretes containing coarse recycled concrete aggregates using multivariate adaptive regression splines (MARS), M5 model tree (M5Tree), and least squares support vector regression (LSSVR) models. *Neural Comput. Appl.* **2020**, *32*, 295–308. [\[CrossRef\]](#)
12. Ho, H.J.; Iizuka, A.; Shibata, E. Chemical recycling and use of various types of concrete waste: A review. *J. Clean Prod.* **2021**, *284*, 124785. [\[CrossRef\]](#)
13. Guerra, B.C.; Leite, F.; Faust, K.M. 4D-BIM to enhance construction waste reuse and recycle planning: Case studies on concrete and drywall waste streams. *Waste Manag.* **2020**, *116*, 79–90. [\[CrossRef\]](#) [\[PubMed\]](#)
14. Mi, R.J.; Pan, G.H.; Liew, K.M.; Kuang, T. Utilizing recycled aggregate concrete in sustainable construction for a required compressive strength ratio. *J. Clean Prod.* **2020**, *276*, 124249. [\[CrossRef\]](#)
15. Xia, B.; Ding, T.; Xiao, J.Z. Life cycle assessment of concrete structures with reuse and recycling strategies: A novel framework and case study. *Waste Manag.* **2020**, *105*, 268–278. [\[CrossRef\]](#) [\[PubMed\]](#)
16. Welsh-Huggins, S.J.; Liel, A.B.; Cook, S.M. Reduce, Reuse, Resilient? Life-Cycle Seismic and Environmental Performance of Buildings with Alternative Concretes. *J. Infrastruct. Syst.* **2020**, *26*, 04019033. [\[CrossRef\]](#)
17. Collivignarelli, C.; Sorlini, S. Reuse of municipal solid wastes incineration fly ashes in concrete mixtures. *Waste Manag.* **2002**, *22*, 909–912. [\[CrossRef\]](#)
18. Hamdi, A.; Abdelaziz, G.; Farhan, K.Z. Scope of reusing waste shredded tires in concrete and cementitious composite materials: A review. *J. Build. Eng.* **2021**, *35*, 102014. [\[CrossRef\]](#)
19. Wu, H.; Liu, C.; Shi, S.; Chen, K. Experimental Research on the Physical and Mechanical Properties of Concrete with Recycled Plastic Aggregates. *J. Renew. Mater.* **2020**, *8*, 727–738. [\[CrossRef\]](#)
20. Dosho, Y. Development of a sustainable concrete waste recycling system—Application of recycled aggregate concrete produced by aggregate replacing method. *J. Adv. Concr. Technol.* **2007**, *5*, 27–42. [\[CrossRef\]](#)
21. Wang, R.X.; Zhang, Y.X. Recycling fresh concrete waste: A review. *Struct Concr.* **2018**, *19*, 1939–1955. [\[CrossRef\]](#)
22. Zhou, Z.; Huang, L.; Jiang, H.; Wen, P.; Zhao, L.; Zhao, Y.; Duan, C.; Luo, Z.; Wang, Z.; Liu, C.; et al. Kinematics of elastic screen surface and elimination mechanism of plugging during dry deep screening of moist coal. *Powder Technol.* **2019**, *346*, 452–461. [\[CrossRef\]](#)
23. Peng, L.; Wang, Z.; Ma, W.; Chen, X.; Zhao, Y.; Liu, C. Dynamic influence of screening coals on a vibrating screen. *Fuel* **2018**, *216*, 484–493. [\[CrossRef\]](#)
24. Jiang, H.; Qiao, J.; Zhou, Z.; Zhao, Y.; Yang, Y.; Duan, C.; Luo, Z.; Cai, L.; Wang, S.; Pan, M. Time evolution of kinematic characteristics of variable-amplitude equal-thickness screen and material distribution during screening process. *Powder Technol.* **2018**, *336*, 350–359. [\[CrossRef\]](#)
25. Wang, W.N.; Duan, C.L.; Jiang, H.S.; Yu, S.J.; Zhou, Z.G.; Qiao, J.P.; Zhao, Y.M.; Pan, M. Mechanism of overcoming plugging and optimization of parameters for rigid-flexible coupled elastic screening of moist fine coal. *Powder Technol.* **2020**, *376*, 113–125. [\[CrossRef\]](#)

26. Zhu, H.P.; Zhou, Z.Y.; Yang, R.Y.; Yu, A.B. Discrete particle simulation of particulate systems: Theoretical developments. *Chem. Eng. Sci.* **2007**, *62*, 3378–3396. [[CrossRef](#)]
27. Harzanagh, A.A.; Orhan, E.C.; Ergun, S.L. Discrete element modelling of vibrating screens. *Min. Eng.* **2018**, *121*, 107–121. [[CrossRef](#)]
28. Zhao, L.L.; Zhao, Y.M.; Bao, C.Y.; Hou, Q.F.; Yu, A.B. Optimisation of a circularly vibrating screen based on DEM simulation and Taguchi orthogonal experimental design. *Powder Technol.* **2017**, *310*, 307–317. [[CrossRef](#)]
29. Li, C.Z.; Honeyands, T.; O’Dea, D.; Moreno-Atanasio, R. DEM study on size segregation and voidage distribution in green bed formed on iron ore sinter strand. *Powder Technol.* **2019**, *356*, 778–789. [[CrossRef](#)]
30. Jimenez-Herrera, N.; Barrios, G.K.P.; Tavares, L.M. Comparison of breakage models in DEM in simulating impact on particle beds. *Adv. Powder Technol.* **2018**, *29*, 692–706. [[CrossRef](#)]
31. George, G.F.F. Hertz’s Miscellaneous Papers. *Nature* **1896**, *55*, 6–9. [[CrossRef](#)]
32. Johnson, K.L.; Kendall, K.; Roberts, A.D. Surface Energy and the Contact of Elastic Solids. *Proc. Math. Phys. Eng. Sci.* **1971**, *324*, 301–313.